



**Improved Performance Induced by in-situ Ligand Exchange
Reactions of Copper Bipyridyl Redox Couples in Dye-
Sensitized Solar Cells**

Journal:	<i>ChemComm</i>
Manuscript ID	CC-COM-09-2018-007191.R1
Article Type:	Communication

SCHOLARONE™
Manuscripts

Improved Performance Induced by *in-situ* Ligand Exchange Reactions of Copper Bipyridyl Redox Couples in Dye-Sensitized Solar Cells

Received 00th January 20xx,
Accepted 00th January 20xx

DOI: 10.1039/x0xx00000x

Yujue Wang^a and Thomas W. Hamann^{*a}

www.rsc.org/

Copper bipyridyl redox couples are interesting mediators for dye-sensitized solar cells (DSSCs). Here we show that the electrolyte additive 4-tert-butylpyridine (TBP) actually substitutes common bidentate ligands on the Cu(II) species to form [Cu(TBP)₄]²⁺, which is a poor electron acceptor and thus allows high voltages and charge collection efficiencies to be achieved.

In the years following Grätzel's breakthrough 1993 report of a 10% efficient dye-sensitized solar cell, DSSC, efforts to further improve the efficiency were stymied by the reliance on the triiodide/iodide (I₃⁻/I⁻) redox shuttle.¹ The major limitation of utilizing I₃⁻/I⁻ stems from the high overpotential necessary for efficient dye regeneration.² Over the past decade, use of outer-sphere redox shuttles have allowed systems to be designed which are capable of reducing this overpotential and improving the performance. Cobalt-based redox shuttles have received the most attention, and DSSCs employing the [Co(bpy)₃]^{3+/2+} (bpy = 2,2'-bipyridine) redox mediator produced a reported efficiency of over 12%.³

DSSCs employing copper-based redox shuttles have been the subject of increasing interest. Copper-based redox shuttles have been investigated in DSSCs as early as 2005.⁴ In that first report, the [Cu(dmp)₂]^{2+/+} (dmp = 2,9-dimethyl-1,10-phenanthroline) redox shuttle showed relatively poor performance due to poor regeneration of N719 which was attributed to the large reorganization energy associated with a distortion of the pseudo-tetrahedral [Cu(dmp)₂]⁺ complex upon oxidation. Interestingly, use of the structurally very similar [Cu(dmbpy)₂]^{2+/+} (dmbpy = 6,6'-dimethyl-2,2'-bipyridine) redox shuttle was recently shown to produce near unity dye regeneration efficiency with only a 0.11 V overpotential when paired with the Y123 dye.^{5,6} Such systems have recently shown very exciting efficiencies of over 13% for liquid electrolytes,

32% under ambient lighting, as well as solid state systems over 11%.⁷ Figure 1 shows a cyclic voltammogram (CV) of [Cu(dmbpy)₂]^{2+/+} with a redox wave at 0.33 V vs. Fc⁺⁰, which agrees with literature reports.⁵ Scan rate dependent CVs, shown in figure S3, indicate that this is a reversible, one-electron redox process. When TBP is included in the electrolyte, to mirror the electrolyte conditions utilized in high efficiency DSSCs, the cathodic return wave is dramatically distorted, with only a minor change observed for the anodic peak.

The slight decrease of the anodic peak current can be due to the increased viscosity with TBP in the solution and decreased diffusion coefficient of the redox species. Kavan et. al have reported that the addition of TBP will slow down the diffusion of the [Cu(dmp)]^{2+/+} couple by measuring the finite-length Warburg diffusion impedance in a symmetrical dummy cell.⁸ While increased viscosity can account for the diminished anodic peak, it cannot account for the transformation of the cathodic wave.

Hupp et al. showed that TBP is not innocent in the redox behavior of the [Cu(PDTO)]^{2+/+} (PDTO = 1,8-bis(2'-pyridyl)-3,6-dithiooctane) redox couple. TBP displaces the tetradentate PDTO ligand on the Cu²⁺ center while PDTO displaces the TBP on the Cu⁺ center.⁹ Such substitutions are in line with prior work on copper redox complexes.¹⁰⁻¹² In order to determine if a similar effect is occurring for the [Cu(dmbpy)₂]^{2+/+} redox couple, TBP

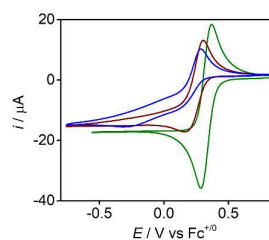


Figure 1. Electrochemical behaviour of [Cu(dmbpy)₂]^{2+/+} in acetonitrile: 4 mM [Cu(dmbpy)₂]²⁺ with the addition of 0 (green), 13 (dark red) and 25 (blue) equivalents of TBP.

^a Department of Chemistry, Michigan State University, 574 S Shaw Lane, East Lansing, USA, 48824

Electronic Supplementary Information (ESI) available: Experimental sections and additional characterization including ¹H NMR, cyclic voltammogram, UV-Vis. Sandwich cell configuration, current voltage measurement and electrochemical impedance spectroscopy measurements. See DOI: 10.1039/x0xx00000x

was titrated in the $[\text{Cu}(\text{dmbpy})_2]^{2+/+}$ electrolyte. After 10 equivalents of TBP were introduced to the electrolyte, the cathodic peak decreased and another peak around -0.4 V appeared. When 25 equivalents of TBP were present, even at high scan rates (ca. 3 V/s) the cathodic peak is dominated by the peak at -0.4 V. This behavior is consistent with the hypothesis that TBP readily displaces the dmbpy ligand once $[\text{Cu}(\text{dmbpy})_2]^+$ is oxidized. In order to test this idea, we independently synthesized the $\text{Cu}(\text{TBP})_4(\text{OTf})_2$ complex (see SI for details).

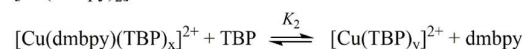
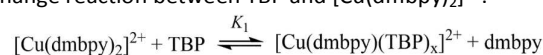
Figure 2a shows the absorption spectra of $[\text{Cu}(\text{dmbpy})_2]^+$, $[\text{Cu}(\text{dmbpy})_2]^{2+}$ and $[\text{Cu}(\text{TBP})_4]^{2+}$ complexes dissolved in acetonitrile. The $[\text{Cu}(\text{TBP})_4]^{2+}$ complex exhibits a weak absorption peak at 580 nm, whereas the $[\text{Cu}(\text{dmbpy})_2]^{2+}$ complex has weak absorption maxima at 724 nm and 1038 nm. Titration of the $[\text{Cu}(\text{dmbpy})_2]^{2+}$ solution with aliquots TBP results in the disappearance of the peak at 1038 nm and an apparent shift of the lower wavelength peak. No isosbestic point is seen, which we attribute to the likely presence of multiple species in solution upon the addition of moderate concentrations of TBP. When 25 or more equivalents of TBP was added, the solution exhibits a nominally identical spectrum as the $[\text{Cu}(\text{TBP})_4]^{2+}$ solution. This result strongly suggests the TBP ligand exchanges with one dmbpy ligand at the Cu^{2+} center at low to intermediate concentrations, and fully displaces it at larger concentrations.

To unambiguously and quantitatively determine the extent of dmbpy displacement by TBP, proton NMR spectra were taken of $[\text{Cu}(\text{dmbpy})_2]^{2+}$ in AcN-d_3 without and with the addition of TBP. Because $[\text{Cu}(\text{dmbpy})_2]^{2+}$ is paramagnetic, the proton signals of the dmbpy ligands coordinated to the Cu^{2+} center show very different chemical shifts than free dmbpy ligands in the solution (figure S2), which allowed determining the concentration of free, i.e. displaced, dmbpy ligands. No evidence of free dmbpy ligand was observed for the neat solutions.

The singlet peak at 5.32 ppm shown on the full ^1H NMR spectrum corresponds to the proton signal of DCM which is used as an internal standard to calibrate the concentration of other protons. The broadened peaks at 13.2, 3.3 and -6.67 ppm are attributed to the ligand coordinated to the paramagnetic Cu^{2+} center. Peaks at 0-1 ppm can be seen upon the introduction of TBP to solution. The absence of distinct

chemical shifts for complexed and free TBP on the spectrum can be attributed to the fast ligand exchange rate between TBP and Cu^{2+} centered complex.¹³ There are three sharp peaks between 7 to 8.5 ppm, which correspond to the aromatic proton signals of the free dmbpy ligand. By integrating the proton signals at 8.07, 7.62 and 7.10 ppm and comparing this to the integrated DCM standard peak area at 5.32 ppm, a ratio of the free ligand to the total Cu^{2+} concentration can be calculated. An increased ratio between free dmbpy and Cu^{2+} was observed during titration. When more than 15 eq. of TBP was added into the solution, the ratio reaches a plateau at a value of 2, which indicates complete replacement of the dmbpy ligand by TBP (figure 3b). Titrations of $[\text{Cu}(\text{dmbpy})_2]^+$ with TBP were also performed and monitored with UV-Vis and NMR, which showed no evidence of ligand exchange.

From the above, there are clearly two steps in the ligand exchange reaction between TBP and $[\text{Cu}(\text{dmbpy})_2]^{2+}$:



The reversibility of these two reactions are established in figure S6 and the preceding text. Unfortunately, equilibrium constants could not be derived; the concentration of free TBP in solution could not be accurately determined because the coordinated and free TBP exchange too fast at room temperature on the NMR time scale to be isolated.

The absorption spectrum of the purported intermediate complex has a strong overlap with $[\text{Cu}(\text{dmbpy})_2]^{2+}$ therefore the absorption of the mixture could not be fitted accurately. However, since the highest reported efficiency DSSCs employ a large excess of TBP in the electrolyte, the equilibrium is pushed to the right where there is minimal coordination of dmbpy to the Cu^{2+} center.

The DSSC electrolytes used to produce the highest efficiencies are generated by mixing 0.2 M $[\text{Cu}(\text{dmbpy})_2]^+$, 0.04 M $[\text{Cu}(\text{dmbpy})_2]^{2+}$ and 0.6 M TBP in acetonitrile with an additional supporting electrolyte. Thus, approximately 15 equivalents of TBP with respect to the Cu^{2+} complex are present and the composition of the relevant redox active species actually consist of 0.2 M $[\text{Cu}(\text{dmbpy})_2]^+$ and 0.04 M $[\text{Cu}(\text{TBP})_4]^{2+}$, with additional free dmbpy and TBP in solution. There are many consequences to this ligand exchange. For one, the formal potential of the

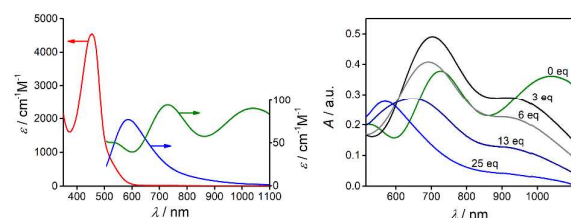


Figure 2. a) Plots of the optical absorption spectra of $[\text{Cu}(\text{dmbpy})_2]^+$ (red), $[\text{Cu}(\text{dmbpy})_2]^{2+}$ (green) and $[\text{Cu}(\text{TBP})_4]^{2+}$ (blue) in acetonitrile. b) Absorption spectra corresponding to the titration of $[\text{Cu}(\text{dmbpy})_2]^{2+}$ with aliquots of TBP in acetonitrile. The base concentration of $[\text{Cu}(\text{dmbpy})_2]^{2+}$ was 4 mM, with 0, 3, 6, 13 and 25 equivalents TBP introduced to the solution.

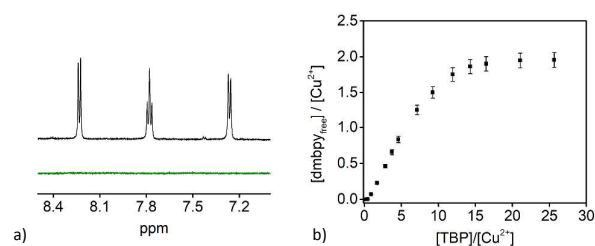


Figure 3. a) Partial proton NMR spectrum of $[\text{Cu}(\text{dmbpy})_2]^{2+}$ with 0 (dark green) and 20 (black) eq. of TBP. Full spectra are provided in figure S7. b) Concentration ratio between detected free dmbpy ligand and the total Cu^{2+} species when different aliquots of TBP were present in the solution. Concentration of dmbpy was determined based on

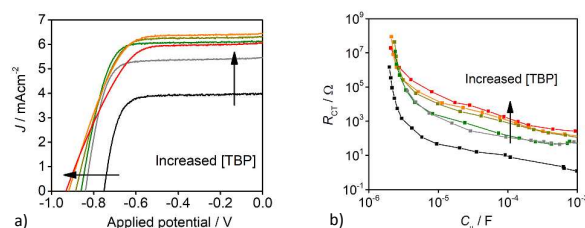
the integration of aromatic proton peaks. Controlled amount of DCM was added as an internal standard for the quantitative calculation.

$[\text{Cu}(\text{dmbpy})_2]^{2+/+}$ redox couple is not a good estimate of the solution potential when TBP is present in the electrolyte, even accounting for the ~ 40 mV shift due to concentration differences in accord with the Nernst equation. Attempts to measure the $[\text{Cu}(\text{TBP})_4]^{2+/+}$ redox potential was thwarted as the complex doesn't exhibit a reversible wave. We therefore measured the solution potential as a function of electrolyte composition. Note that this corresponds roughly to the reference potential in a DSSC in a 2-electrode sandwich cell configuration, as shown in table S1. Addition of TBP to the electrolyte induced a negative shift of the solution potential by 270 mV. This negative shift of the solution potential with the addition of TBP represents a loss of voltage of the cell and thus efficiency. We note that a similar effect was shown by Hupp *et al.* upon addition of TBP to solutions of $[\text{Cu}(\text{PDTO})]^{2+/+}$.

Given this loss in reference potential, it is striking that such large open circuit photovoltages, V_{OC} , have been reported for DSSCs employing $[\text{Cu}(\text{dmbpy})_2]^{2+/+}$. We prepared cells using the same electrolyte compositions discussed above. Photocurrent density vs applied voltage (J - V) curves were measured and shown in figure 4a. It is interesting to note that the short circuit photocurrent density, J_{SC} , increases significantly upon the introduction of TBP to the electrolyte. Since the TBP should not increase the light harvesting, injection or regeneration processes, we attribute the increased J_{SC} to an improved charge collection efficiency from reduced recombination. This is consistent with the concomitant ~ 200 mV larger V_{OC} observed in the presence of TBP. Since the V_{OC} is the difference in solution potential and Fermi level (E_{F}) in TiO_2 , and the solution potential is shifted ~ 270 mV negative with the addition of TBP, the E_{F} is shifted by ~ 470 mV upon the addition of TBP. The E_{F} is determined by the conduction band edge and recombination kinetics; thus there is either a negative shift of conduction band edge, reduced recombination kinetics, or both, upon the introduction of TBP. It is well known that TBP shifts conduction band edge to more negative values.¹⁴ Addition of TBP induces a shift of the chemical capacitance of cells employing the chemically inert $[\text{Co}(\text{bpy})_3]^{3+/2+}$ redox shuttle by roughly 200 mV (figure S10), which is in agreement with reports using I_3^-/I^- .¹⁵ Thus, as much as a ~ 270 mV increase in E_{F} should be due to reduced recombination.

To isolate the effect of TBP on the energetics of the semiconductor. The recombination process was measured by electrochemical impedance spectroscopy (EIS) under dark condition. The resultant spectra were fitted using the equivalent circuit displayed in figure S9. The charge transfer resistance (R_{CT}) is plotted versus the chemical capacitance (C_{μ}) in figure 4b. Since the density and distribution of trap states is constant upon surface modification, C_{μ} can be used as an internal standard of the electrochemical potential of electrons in TiO_2 and used to compare relative rate constants of recombination reflected in R_{CT} .^{16,17} Upon addition of TBP to the electrolyte, R_{CT} increases by a factor of ~ 500 under the same electrochemical potential of electrons (C_{μ}). The slower rate of

electron recombination agrees with our proposed ligand exchange reaction in the electrolyte when TBP is present. In



other words, addition of TBP replaces the fast electron acceptor

Figure 4. a) Plots of J - V curves for DSSCs employing different concentrations of TBP to the electrolyte. b) Plots of the charge transfer resistance (R_{CT}) vs the chemical capacitance (C_{μ}) of DSSCs to show the effect of TBP on recombination kinetics. Plots are color-coded according to concentrations of TBP in the electrolyte: 0 M (black), 0.1 M (gray), 0.2 M (green), 0.3 M (dark yellow), 0.4 M (orange) and 0.5 M (red).

$[\text{Cu}(\text{dmbpy})_2]^{2+}$ with the worse electron acceptor $[\text{Cu}(\text{TBP})_4]^{2+}$ that manifests in slower recombination (higher R_{CT}). The ~ 500 times slower recombination is consistent with a 270 mV higher E_{F} , as well as the larger open circuit photovoltages and charge collection efficiencies.

The results presented above explain the excellent performance of the recently reported DSSCs employing $[\text{Cu}(\text{dmbpy})_2]^{2+/+}$ electrolytes, and the critical role of TBP. We showed that the addition of TBP to $[\text{Cu}(\text{dmbpy})_2]^{2+/+}$ electrolytes results in a rapid ligand substitution reaction to form the $[\text{Cu}(\text{TBP})_4]^{2+/+}/[\text{Cu}(\text{dmbpy})_2]^+$ redox species in solution. The $[\text{Cu}(\text{dmbpy})_2]^+$ species has previously been shown to quantitatively regenerate dyes with minimal driving force (ca. 0.1 V), which is critical in achieving high efficiencies. The consequence of the substitution reaction is that recombination is reduced which further improves both the V_{OC} and J_{SC} . Interestingly, the ligand exchange reaction also induces a negative shift of the solution potential, which results in a ~ 270 mV loss in V_{OC} . Thus, optimization of the ligand substitution product solution potential offers a path to further improve the photovoltage by over 200 mV without concomitant loss in photocurrent. Finally, we note that the recent reports of high efficiency solid-state DSSCs also contain TBP, which we believe is critical to the excellent performance.¹⁸ Work is ongoing in our lab to elucidate the effect of TBP on these very interesting solid-state systems.

This work was supported by the Chemical Sciences, Geosciences, and Biosciences Division, Office of Basic Energy Sciences, Office of Science, the U.S. Department of Energy Grant No. DE-SC0017342.

Conflicts of interest

There are no conflicts to declare.

Notes and references

- 1 Nazeeruddin, M. K.; Kay, A.; Rodicio, I.; Humphry-Baker, R.; Mueller, E.; Liska, P.; Vlachopoulos, N.; Graetzel, M., *J. Am. Chem. Soc.*, 1993, **115**, 6382.
- 2 Boschloo, G.; Hagfeldt, A., *Acc. Chem. Res.*, 2009, **42**, 1819.
- 3 Yella, A.; Lee, H.-W.; Tsao, H. N.; Yi, C.; Chandiran, A. K.; Nazeeruddin, M. K.; Diau, E. W.-G.; Yeh, C.-Y.; Zakeeruddin, S. M.; Grätzel, M., *Science*, 2011, **334**, 629.
- 4 Hattori, S.; Wada, Y.; Yanagida, S.; Fukuzumi, S., *J. Am. Chem. Soc.*, 2005, **127**, 9648.
- 5 Li, J.; Yang, X.; Yu, Z.; Gurzadyan, G. G.; Cheng, M.; Zhang, F.; Cong, J.; Wang, W.; Wang, H.; Li, X.; Kloo, L.; Wang, M.; Sun, L., *RSC Adv.*, 2017, **7**, 4611.
- 6 Saygili, Y.; Söderberg, M.; Pellet, N.; Giordano, F.; Cao, Y.; Muñoz-García, A. B.; Zakeeruddin, S. M.; Vlachopoulos, N.; Pavone, M.; Boschloo, G.; Kavan, L.; Moser, J.-E.; Grätzel, M.; Hagfeldt, A.; Freitag, M., *J. Am. Chem. Soc.*, 2016, **138**, 15087.
- 7 Cao, Y.; Liu, Y.; Zakeeruddin, S. M.; Hagfeldt, A.; Grätzel, M., *Joule*, 2018, **2**, 1108.
- 8 Kavan, L.; Saygili, Y.; Freitag, M.; Zakeeruddin, S. M.; Hagfeldt, A.; Grätzel, M., *Electrochim. Acta*, 2017, **227**, 194.
- 9 Hoffeditz, W. L.; Katz, M. J.; Deria, P.; Cutsail III, G. E.; Pellin, M. J.; Farha, O. K.; Hupp, J. T., *J. Phys. Chem. C*, 2016, **120**, 3731.
- 10 Miller, M. T.; Gantzel, P. K.; Karpishin, T. B., *Inorg. Chem.*, 1998, **37**, 2285.
- 11 Kavana, M.; Powell, D. R.; Burstyn, J. N., *Inorganica Chim. Acta*, 2000, **297**, 351.
- 12 Razgoniaev, A. O.; McCusker, C. E.; Castellano, F. N.; Ostrowski, A. D., *ACS Macro Lett.*, 2017, **6**, 920.
- 13 Forsberg, J. H.; Dolter, T. J.; Carter, A. M.; Singh, D.; Aubuchon, S. A.; Timperman, A. T.; Ziaee, A., *Inorg. Chem.*, 1992, **31**, 5555.
- 14 Haque, S. A.; Palomares, E.; Cho, B. M.; Green, A. N. M.; Hirata, N.; Klug, D. R.; Durrant, J. R., *J. Am. Chem. Soc.*, 2005, **127**, 3456.
- 15 Yin, X.; Zhao, H.; Chen, L.; Tan, W.; Zhang, J.; Weng, Y.; Shuai, Z.; Xiao, X.; Zhou, X.; Li, X.; Lin, Y., *Surf. Interface Anal.*, 2007, **39**, 809.
- 16 Fabregat-Santiago, F.; Garcia-Belmonte, G.; Mora-Seró, I.; Bisquert, J., *Phys. Chem. Chem. Phys.*, 2011, **13**, 9083.
- 17 Bisquert, J., *Phys. Chem. Chem. Phys.*, 2003, **5**, 5360.
- 18 Zhang, W.; Wu, Y.; Bahng, H. W.; Cao, Y.; Yi, C.; Saygili, Y.; Luo, J.; Liu, Y.; Kavan, L.; Moser, J.-E.; Hagfeldt, A.; Tian, H.; Zakeeruddin, S. M.; Zhu, W.-H.; Grätzel, M., *Energy Environ. Sci.*, 2018, **11**, 1779.